The novel curcumin analogue AKT-100 targets mutant p53 in gynecologic cancer cells

Geneva L. Williams,[1] Lane E. Smith,[1] Jamie L. Padilla,[1] Alexander S. Goss,[1] Daisy Belmares-Ortega,[1] Xiangxiang Wu,[1] Jennifer N. Daw,[1] Sumegha Mitra,[1] Prakash Jagtap,[2] Jun-young Choe,[3] and Kimberly K. Leslie[1,4]

1. University of New Mexico Health Sciences Center, Albuquerque, NM 87131
2. Akkadian Therapeutics, Stoneham, MA 02180
3. University of New Mexico Main Campus, Albuquerque, NM 87131
4. To whom correspondence should be addressed

Running Title: Curcumin analogue AKT-100 targets mutant p53 in gynecologic cancers

Key Words: Ovarian cancer, endometrial cancer, curcumin, AKT-100, olaparib, HO-3867, p53

The authors declare no potential conflicts of interest.

Graphical Abstract:

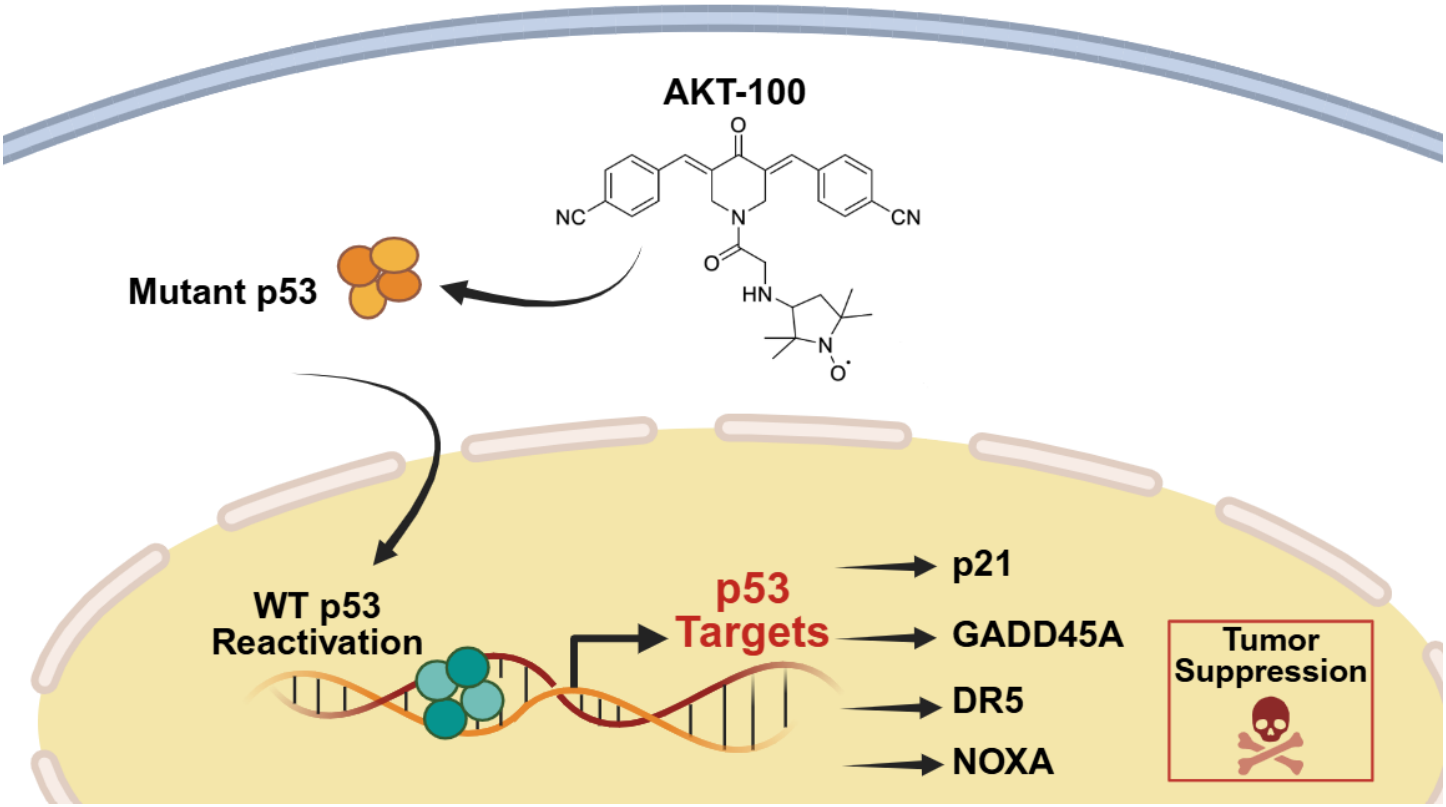

Abstract

Loss of the normal tumor suppressive functions of p53, the “guardian of the genome,” is common in advanced cancers. Mutations in *TP53* occur in various ways which can result in p53 null tumor cells as well as in tumor cells highly expressing missense, gain of oncogenic function p53 proteins. Gain of function p53 proteins not only lose wild type p53 pro-apoptotic and DNA repair functions, but gain novel oncogenic functions. We hypothesize that directly targeting missense mutant p53 instead of downstream pathways has substantial advantages. Analogues of curcumin have been reported to bind mutant p53 to accomplish this goal. In this report, we developed a series of novel molecules derived from the curcumin backbone. We identified a particularly active curcumin analogue, AKT-100, and demonstrate binding to mutant p53 proteins to reinstate p53 wild type functionality. This agent exhibits impressive cell killing in multiple ovarian and serous endometrial cancer cells at concentrations ranging from 100-300 nM. AKT-100 is also synergistic with the PARP inhibitor olaparib and with chemotherapy by inhibiting alternative DNA repair mechanisms associated with resistance to standard therapies. RNA sequencing confirms that AKT-100 reactivates wild type p53-driven expression of genes associated with normal cell cycle regulation (induction of *CDKN1A* encoding p21 and *GADD45A*), apoptosis (induction of *PMAIP1* encoding Noxa and *DR5* encoding Death Receptor 5), and inhibits DNA replication and repair in cancer cells. Thus, p53 reactivators under development, such as AKT-100, hold promise as novel therapeutic agents to directly target missense mutant, gain of oncogenic function p53.

Introduction

It is well established that mutations in *TP53*, the gene encoding p53, are shared by most types of human tumors, and these mutations enhance cancer cell growth and survival (1). The evolutionary emergence of p53 homologues is associated with multicellularity, when genome maintenance became a specialized task. Human p53 was discovered more than 40 years ago in the Arnold J. Levine laboratory (2). Initially characterized as a tetrameric transcription factor, normal wild type (WT) p53 also modulates the activity of other factors directly through protein/protein interactions and through DNA binding. It binds to DNA at specific response elements and globally to identify DNA breaks and initiate repair – if repair is not possible, apoptosis is induced (3). Expressed at low, tightly controlled levels in normal cells, p53 is often not expressed (null) or conversely, missense mutated and highly over-expressed in cancer (4-6).

We propose that identifying agents that bind to and inhibit the oncogenic properties of missense mutated p53 would be a therapeutically efficacious strategy to prevent and to treat many cancers. Also, mutations in *TP53* comprise some of the very first alterations in the process of oncogenesis, indicating that targeting these mutant proteins could be a major step towards preventing cancer as well as treating resultant tumors. Importantly, recurrent, missense single amino acid alterations in p53 not only cause the loss of wild type tumor suppression, but result in the acquisition of new oncogenic functionality wherein mutant forms of p53 disrupt nearly all of the normal processes of the cell (7-11). Indeed, the “guardian of the genome” morphs into the “guardian of the cancer cell” (12-14).

The most aggressive and lethal gynecologic malignancies, including uterine serous endometrial cancer and high grade serous ovarian cancer, are characterized by mutations in *TP53* and often highly express the missense mutated forms of the protein that are fundamental to oncogenesis and tumor progression (5, 6, 15). Importantly, the identical single amino acid hotspot p53 mutations, comprising about eight unique, recurrent alterations, occur over and over again in all cancers. These constitute a set of oncogenic “gain of function” proteins that are potentially targetable with p53 reactivator strategies. However, to date, effective p53 reactivator therapies have yet to reach widespread clinical practice. The lack of effective therapeutic options for such p53-mutant cancers constitutes a major gap in medical knowledge and the clinical armamentarium (16).

Gain of oncogenic function mutant p53 oncoproteins significantly enhance angiogenesis (17), inhibit T-cell tumor recognition and permit the over-expression of oncogenes such as *Myc* (8, 18, 19). Based upon preclinical data and with in-depth analyses of clinical studies including GOG 86P (5, 6), NRG GY018 (20) and RUBY (21), mutant p53 has been confirmed as a marker for sensitivity to bevacizumab (anti-VEGFA), pembrolizumab (anti-PD-1) and dostarlimab (anti-PD-1) with significant improvements in both progression free survival (PFS) and overall survival (OS) when added to chemotherapy compared to chemotherapy alone in advanced endometrial cancers. Yet in addition to adding downstream mutant p53-mediated pathway blocking targeted agents to chemotherapy, another therapeutic opportunity would be to target mutant p53 directly, re-establishing the wild type pro-apoptotic functionality as a means to inhibit cancer cell proliferation. Curcumin analogues such as HO-3867 are reported to bind to mutant forms of p53 as well as to STAT3, another important oncogenic driver when over-active, and to inhibit cancer cell proliferation (22-24). Herein, we synthesized a new curcumin analogue, AKT-100, with structural similarities to HO-3867 as well as a series of additional derivatives, AKT-109, 111, 115 and 121. We sought to identify one or more molecules that bind to p53 and reinstate its wild type tumor suppressive activities.

Curcumin itself is widely used as a spice in India and other near Eastern countries which report some of the lowest bowel cancer incidences in the world. It is well known as an anti-inflammatory, anti-angiogenic and anti-oxidant molecule with anti-cancer activity (25, 26). While curcumin is non-toxic and has been extensively used for medicinal purposes; it is not highly soluble and is poorly absorbed systemically from the gut epithelium. Hence there is a need and an opportunity to create and test curcumin analogues with enhanced solubility for future drug development (27-29).

Opportunities to utilize effective curcumin analogues could range from single agent treatment of malignancies, prophylaxis against cancer development in vulnerable populations, and/or enhancing the activity of standard therapies when given in combination. For example, poly (ADP-ribose) polymerase (PARP) inhibitors commonly used in maintenance for ovarian cancer are most effective in tumors with defects in homologous recombination DNA repair. However, resistance develops when homologous recombination is reconstituted by reversion mutations or other means in cells when exposed to therapy (30). Inhibition of homologous recombination and other DNA repair pathways utilized by cancer cells to escape PARP inhibitor

sensitivity by a second agent, such as a curcumin analogue, is a potential mechanism to forestall or reverse PARP inhibitor resistance (31, 32). The same mechanism of tumor DNA repair inhibition could also enhance the sensitivity of tumor cells to chemotherapy. Given the myriad of potential anti-cancer mechanisms of action of curcumin and its analogues, we set out to identify novel therapeutic molecules and to assess their actions and activities.

Materials and Methods

Synthesis of AKT-100: In collaboration with Akkadian Therapeutics (AKTX, Stoneham, MA), we have identified derivatives of the curcumin analogue HO-3867, such as AKT-100, as ligands that bind to p53. AKT-100 is derived from HO-3867 by removing the toxic functional groups such as tertiary and allyl amines (Figure 1A), which induce the human Ether-à-go-go-Related Gene (hERG) channel blocker activity of HO-3867. The absorption, distribution, metabolism, and excretion (ADME) and drug-like properties of HO-3867 were determined using the computational tool STARDROP (33). The hERG pIC_{50} value of HO-3867 is 6.94 (33). An ideal hERG pIC_{50} value should be <5 for consideration as a safer drug candidate. The proxylamino group on AKT-100 would be expected to satisfy the main pharmaceutical objectives, conferring aqueous solubility (necessary for oral bioavailability, salt formation and oral formulations), and providing long-lasting effects. To identify a highly effective and bioavailable analogue for eventual clinical use, we have designed a library of AKT-100 derivatives which can be tested to identify one or more optimal compounds. Synthetic pathways for the synthesis of AKT-100, AKT-111, AKT-121, AKT-109 and AKT-115 are displayed in Scheme 1 and 2 (Supplemental Figure 1), and synthetic procedures are described in Supplemental Experimental Section. All solvents, reagents and starting materials (i.e. Compound # 1, 2, 3, 4, 12, 14, 15 and 18) required for the synthesis of AKT compounds, were purchased from Sigma-Aldrich, USA. 2-Fluoro-5-((4-oxo-3,4-dihydrophthalazin-1-yl) methyl) benzoic acid (compound # 8, CAS No.: 763114-26-7) for the synthesis of AKT-121(33) was purchased from Ambeed (Buffalo Grove, IL 60089, USA). Proton nuclear magnetic resonance (^{1}H-NMR) spectra were obtained from Varian 300 MHz spectrophotometer. Thin layer chromatography (TLC) was carried out on precoated TLC plates with silica gel 60 F-254 and preparative TLC on precoated Whatman 60A TLC plates. ^{1}H-NMR of the paramagnetic nitroxide compounds were significantly shifted, and spectral lines were broadened due to the unpaired electron's magnetic moment. The final compounds were analyzed by mass spectral (MS) analysis data.

Flash column chromatography was performed with Merck ultra-pure silica gel (Darmstadt, Germany, 230–400 mesh). Analytical HPLC was performed using a Waters Alliance 2795 series system, equipped with a Waters UV 2996PAD (set at 254 nM) and Micromass MS Quattro LC detector or using Waters Alliance 2690 series system, equipped with the Micromass LCT detector. A YMC-Pack-ODS-AQ (series AQ12505-1546WT, size 150 mm X 4.6 mm, S-5 µM) column was used. A gradient mobile phase starting with 70% water with 0.05% ammonium formate and 30% methanol with 0.05% ammonium formate was employed with a flow rate of 0.8 mL/min. Based on the UV and MS detectors, all final compounds evaluated in the *in vitro* assays showed HPLC purity >95%.

Protein purification: The plasmid encoding the human p53 core domain (residues 94–312; AddGene plasmid #24866;(34)) was used as the template. Site-directed mutagenesis was performed using the QuikChange protocol (35) and the resulting constructs were sequence-verified at the University of Chicago Sanger Sequencing Core. The verified plasmid was transformed into *E. coli* C41 cells (36), which were cultured in LB medium. From 10 L of *E. coli* culture, ~50 mg of p53 protein with ~80% purity was typically obtained. Purification was carried out using a single step with a Talon (Takara, Kyoto, Japan) affinity column. When the initial purity was below 80%, an additional size-exclusion chromatography step on a Superdex 200 column (Cytiva, Marlborough, MA) was performed. Protein purity was quantified using ImageJ.

Isothermal Titration Calorimetry (ITC): ITC was performed on a Nano ITC instrument (TA Instruments, New Castle, DE) at 25 °C. Purified p53 core domain (residues 94–312), and its variants were extensively dialyzed against ITC buffer (50 mM sodium phosphate, pH 7.4, 150 mM NaCl, 1 mM DTT) and degassed immediately before use. The sample cell (300 µL) was loaded with 10 µM p53 protein, while the syringe (50 µL) was filled with 150 µM AKT-100. Each titration consisted of 25 injections of 2 µL with 200 second intervals, under continuous stirring at 300 rpm. Thermograms were integrated, baseline-corrected, and analyzed using NanoAnalyze software (TA Instruments). Binding parameters, including stoichiometry (n), equilibrium dissociation constant (Kd), enthalpy change (ΔH), and entropy contribution (ΔS), were obtained by fitting the data to a multiple site binding model.

Thermal shift assay (TSA) with SYPRO orange: The fluorescence probe SYPRO orange (λ excitation 490 nm and λ emission 585 nm) binds preferentially to unfolded segments of proteins, and its fluorescence correlates with the degree of protein unfolding (SYPRO orange alone is non-fluorescent). Increasing the sample temperature leads to more protein unfolding which, in turn, is determined as an increase in the fluorescence signal of SYPRO orange. This thermal denaturation assay enables convenient determination of protein melting temperatures using multi-well formats and real-time PCR thermal cyclers (37-39). For each reaction, 5 µg (0.02 mM) of protein was mixed with 10 µM SYPRO Orange in 384-well plates, and fluorescence changes were recorded on a ThermoFisher Studio 6 real-time PCR system. The melting temperature (T_m) was determined by fitting the fluorescence-versus-temperature curve to a Boltzmann sigmoidal function in GraphPad Prism.

Fluorescence quenching: Ligand binding perturbs the local environment of tyrosine residues, resulting in decreased intrinsic fluorescence (quenching). Fluorescence changes were monitored as a function of ligand concentration to generate a binding isotherm and determine the dissociation constant (Kd). The experiments shown in Supplemental Figure 2C and D were performed on a Shimadzu RF6000 spectrofluorometer using a single cuvette with excitation at 280 nm. The protein concentration was 0.5 µM.

Cell Culture: KLE (ATCC # CRL-1622) and OVCAR3 (Cat# HTB-161) cells were obtained from ATCC and grown in RPMI 1640 medium (Gibco Cat# 11875-085 or Corning Cat# 10-040-CV) containing 20% FBS (Gibco Ref# A5670701 or Sigma-Aldrich Cat# 12306C-500ML), 1% penicillin-streptomycin (Gibco Ref# 15140-122), and 1% MEM NEAA (Gibco, Ref# 11140-050). COV362 cells (Sigma Aldrich Cat# 07,071,910) were maintained with DMEM (Gibco Ref# 11965-084) containing 10% FBS and 2 mM glutamine (Gibco Cat# 25030-081). Ishikawa, ECC-1, Hec50co cells (gifts from Dr. Erlio Gurpide, New York University), PEO1 (obtained from Dr. Elizabeth Swisher, University of Washington) and PEO4 (Sigma Aldrich Cat # 10,032,309) cells were grown in DMEM containing 10% FBS and 1% penicillin-streptomycin. AN3CA (ATCC #HTB-111) cells were grown in MEM (Gibco Ref# 11095-080) containing 10% FBS and 1% penicillin-streptomycin. As described by Smith *et al.*, all cells were validated and tested periodically for *Mycoplasma* contamination (40). All cells were grown and maintained at 37°C, 5% CO_2 and used for fewer than 10 passages for experiments.

CyQuant Cell Proliferation Assay: Assays were performed as previously described by Smith *et al.* (40) with increasing concentrations of HO-3867 (Selleckchem Cat. #S7501, CAS No. 1172133-28-6), AKT-100 or derivatives AKT-109, AKT-111, AKT-115, and AKT-121 (obtained from AKTX) in fresh media and 100 µL added to triplicate wells. Assays requiring olaparib (Cayman Chemical #10621, CAS No. 763113-22-0) were first drugged with increasing concentrations to determine the IC_{50} in OVCAR3 and COV362 cells. Combined drugging with AKT-100 was then completed using previously obtained AKT-100 IC_{50} values with increasing concentrations of olaparib. Reverse combination assays held olaparib constant at its determined IC_{50} while increasing AKT-100. Proliferation assays using paclitaxel (Cayman Chemical #10461, CAS No. 33069-62-4) were drugged with increasing concentrations to determine the IC_{50} in KLE cells. Combination drugging with AKT-100 was done by maintaining AKT-100 constant at its IC_{50} concentration while increasing paclitaxel. Reverse combination drugging held paclitaxel constant at the previously determined IC_{50} in the presence of increasing concentrations of AKT-100. For experiments using carboplatin (Cayman Chemical #13112, CAS No. 41575-94-4), cells were incubated with increasing concentrations to obtain the IC_{50} value in KLE cells. Combination drugging held one drug constant at the determined IC_{50} value while increasing the other. Graphpad Prism software was used to obtain all IC_{50} values from fluorescence (excitation 485 nm, emission 530 nm) readouts and combinatorial indices were calculated where relevant for combination drugging. All drug treatments were performed in triplicate with two or three independently repeated experiments to confirm results.

RNA Sequencing and Analysis: Cell seeding, RNA collection, sequencing and analysis were completed as previously described by Smith *et al.* (40). Each cell line (Hec50co, Ishikawa, KLE, AN3CA, COV362 and OVCAR3) was treated with AKT-100 at its approximate IC_{50} value (0.50, 0.50, 2.0, 0.10, 0.50, 1.0 µM, respectively) for 24 hours prior to RNA extraction. All samples were processed by the Analytical and Translational Genomics Core at the University of New Mexico. WEB-based GEne SeT AnaLysis Toolkit (WebGestalt) software was used to identify significantly altered pathways using differentially expressed genes. Graphpad Prism software was used to assemble heatmaps displayed in Figure 4B, D and E using Log_2 fold

change values. Additionally, KLE, COV362 and OVCAR3 cells were treated with HO-3867 at their approximate IC_{50} values (4.0, 3.0, and 3.0 µM, respectively) for 24 hours prior to RNA extraction.

Statistical Analyses: IC_{50} values from the cell lines were determined using GraphPad Prism software, version 9.3.1, by applying a nonlinear regression analysis (*[Inhibitor] vs. normalized response* curve) on the normalized fluorescent values.

Results

Novel curcumin analogue AKT-100 binds wild-type and mutant p53 protein.

As displayed in Figure 1A and B, AKTX has synthesized the compounds to feature combinations of multiple double bonds, acting as Michael acceptors or interacting with cysteine residues. Our aim in developing these compounds was to maintain their efficacy as well as to address some of the following: (i) increased water solubility; (ii) improved oral drug delivery; and (iii) improved DMPK parameters. AKTX synthesized multiple analogues for our preclinical validation studies, performing pharmacokinetic (PK) and pharmacodynamic (PD) studies to optimize dosing and administration of lead molecules.

We compared the chemical properties and chemical structures of AKT-100 and other AKT derivatives with HO-3867 for their solubility and oral bioavailability (Figure 1B). The essential parameters to predict molecular solubility and cell membrane permeability for optimizing *in vivo* absorption, such as lipophilicity (LogP), topological polar surface area (TPSA) and molecular weight (MW) were within the optimal range. The desired optimal range of the chemical properties are listed in parentheses in Figure 1B (41, 42). TPSA values help determine a molecule's surface area polarity where higher values are indicative of increased polarity with decreased lipophilicity and overall poor membrane permeability. In addition, a molecule's optimal molecular weight should be less than 500 g/mol and LogP value less than 5 to achieve desirable oral bioavailability (43). LogP values show that AKT-100 and its derivatives are less than 5 with variable molecular weight's, indicating potential for increased bioavailability compared to HO-3867. Also displayed in Figure 1B are the chemical structures of AKT-100 derivatives used in our studies to identify the most effective compound that both binds to mutant p53 to reinstate the normal conformation with normal, pro-apoptotic gene transcription and tumor suppression before leading to future *in vivo* experiments.

To validate the lead compound, AKT-100, for binding to the wild type p53 compared to the most common, recurrent mutant forms of p53 (R175H, Y220C, G244D, R248Q, R273H, D281H), we used ITC, the protein melting temperature and protein fluorescence. Purified wild-type or mutant p53 protein was obtained as described in the methods section and confirmed by SDS PAGE analysis (Supplemental Figure 2A). ITC is a biophysical, label-free analytical technique for determining the binding of molecules in solution (44, 45). The ITC instrument measures the change in the energy of two given interacting molecules as the heat release in the solution, allowing quantitative determination of thermodynamic parameters such as: enthalpy (H), entropy (ΔS), and Gibbs free energy (ΔG), and the equilibrium association constant (Ka), from which the equilibrium dissociation constant Kd can be calculated. ITC data (Supplemental Figure 2B) showed that AKT-100 binds p53 with dissociation constants (Kd) of 5.1 µM and 523 µM, consistent with a multiple sites binding model. The interaction is endothermal, with a predicted stoichiometry of 0.6 and 0.9 (ligand to protein), which reflects sequential ligand binding events and protein dimerization.

Next, the fluorescence probe SYPRO orange was used to determine the protein melting temperature (Tm, denaturation midpoint) as Tm changes upon incubation with a prospective ligand indicate ligand binding (37, 38, 46). The melting temperature of p53 WT and mutants (G244D, R248Q, R273H) decreased upon incubation with AKT-100 or HO-3867 (Figure 1C and D). However, the Tm of mutant p53 variant Y220C increased, possibly indicating greater thermodynamic stability.

Fluorescence quenching is a method to check ligand binding using protein fluorescent residues, such as tryptophan (Trp), tyrosine (Tyr), or phenylalanine (Phe). The changes in the environment of the fluorescent residue induced by ligand binding alters the fluorescence signal (47-50). The core domain of p53 has one Trp, eight Tyr and nine Phe residues. Supplemental Figure 2C shows an emission signal of p53 at 308 nm after sample excitation at 280 nm; the addition of the ligand decreases the emission signal in a concentration-dependent manner. The resulting Kd values from the nonlinear regression fit of the data were 9.8 ± 0.1 µM, 10.8 ± 0.1 µM, and 11.4 ± 0.1 µM, for the p53 WT, G220D and Y244D, respectively (Supplemental Figure 2D).

Thus, we have demonstrated binding of AKT-100 to both WT and mutant p53 proteins indicating target specificity. Our next step was to demonstrate drug efficacy in cancer cell models and the re-establishment of many functional elements of WT p53, such as cancer cell cycle arrest and induction of the pro-apoptotic transcriptome.

A

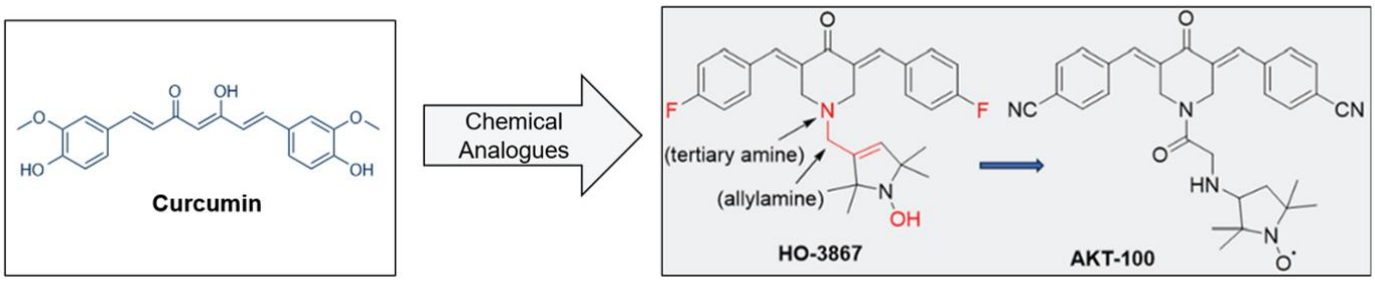

B

In-silico comparison of chemical properties of HO3867 and AKT analogues

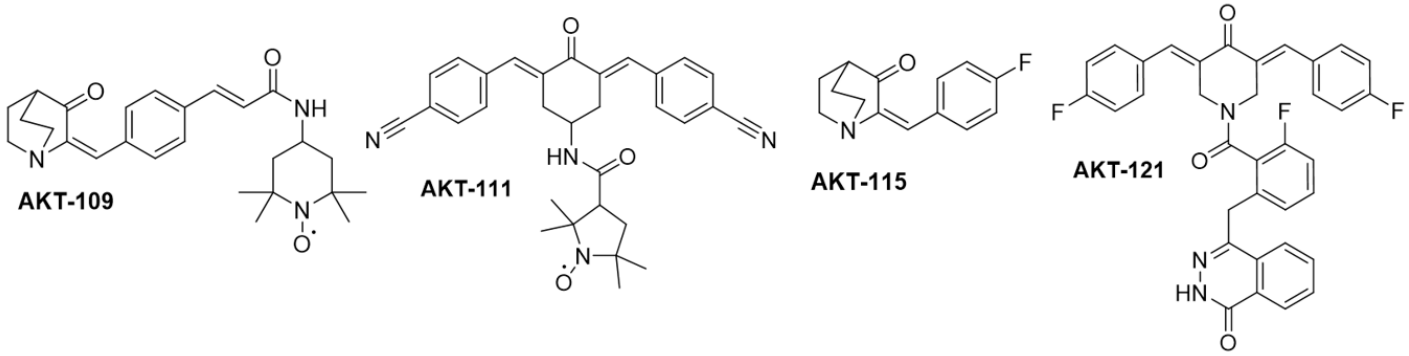

Properties (Desirable range)	HO-3867	AKT-100	AKT-109	AKT-111	AKT-115	AKT-121
LogP (<5)	5.93	3.87	3.29	4.06	1.5	5.7
TPSA (<140 A)	43.77	120.46	72.55	116.8	20.3	83.1
MW (<500 Da)	464.56	523.64	436.26	507.61	231.27	591.59
O & N (<10)	4	8	6	7	2	6
OH &NH (<5)	1	2	2	2	0	1
Violations (0)	1	1	0	1	0	2
Rotatable bonds (<10)	4	5	5	5	1	5

C

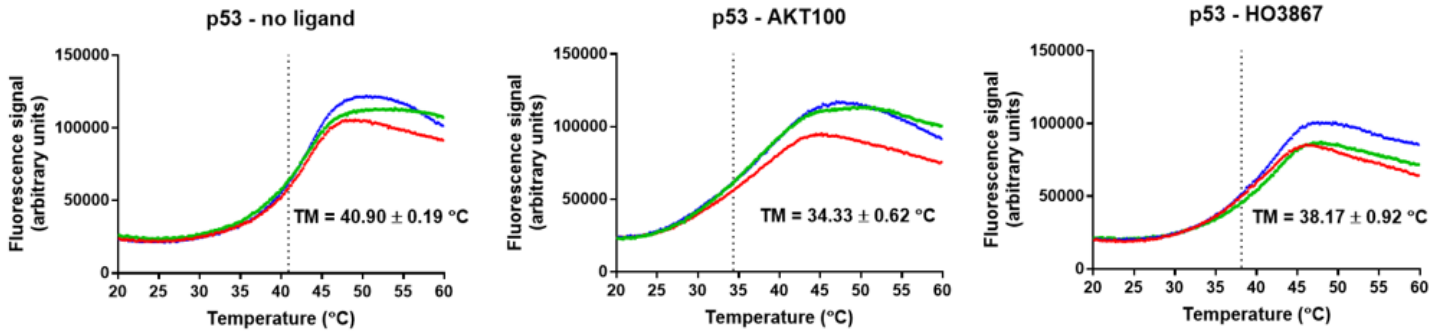

D

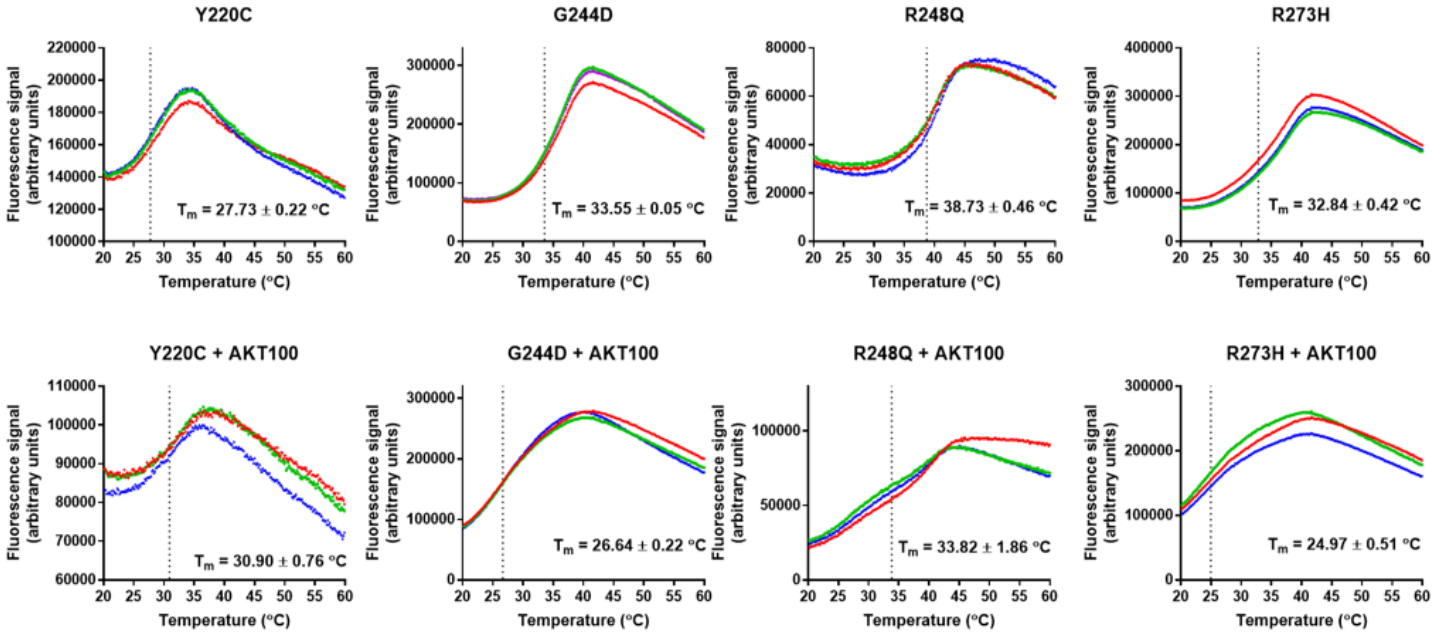

Figure 1. Novel curcumin analogue AKT-100 binds wild-type and mutant p53 protein. (A) Chemical structure of curcumin and the derivation of novel curcumin analogue AKT-100 from HO-3867. **(B)** Chemical structures of AKT-100 analogues AKT-109, AKT-111, AKT-115 and AKT-121. The chart compares values for all compounds demonstrating favorable *in silico* drug-like properties for solubility and activity compared to HO-3867 and AKT-100. **(C)** Fluorescence changes of SYPRO orange incubated with wild-type p53 at different temperatures: p53 alone (left), p53 with AKT-100 (middle), p53 with HO3867 (right). **(D)** Fluorescence changes of SYPRO orange incubated with p53 mutants (Y220C, G244D, R248Q, R273H) at different temperatures: p53 mutants alone (top panels), p53 mutants with AKT-100 (lower panels).

<u>AKT-100 is more therapeutically effective compared to HO-3867 in multiple cell models.</u>

Cell proliferation assays identified IC_{50} values in the low µM - nM range for both AKT-100 and the parent molecule HO-3867 in ovarian and endometrial cancer cell lines harboring p53 mutations. According to Figure 2A and 2B, six cell lines had IC_{50} values ranging from 4-390 nM. Figures 2C-G compare HO-3867 versus AKT-100 treatments in PEO1, ECC-1, KLE, COV362 and OVCAR3 cells, with graphs displaying growth inhibition at lower concentrations of AKT-100. These data demonstrate the effectiveness of novel curcumin analogue AKT-100, however we further asked whether other AKT derivatives are effective at killing cells in our cell models of interest.

A

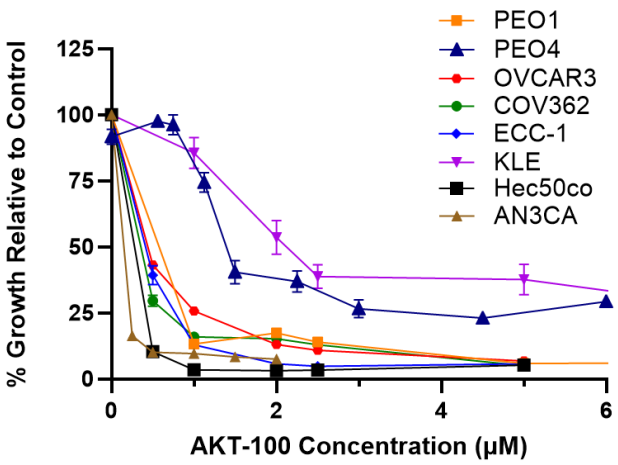

B

	Cell Line	TP53 Mutation	AKT-100 IC_{50} (μM)
Ovarian	PEO1	G244D	0.20
	PEO4	G244D	1.94
	OVCAR3	R248Q	0.39
	COV362	Y220C	0.14
Endometrial	ECC-1	M246V	0.38
	KLE	R175H	2.51
	Hec50co	G187-E224Δ	0.01
	AN3CA	R213Q	0.004

C

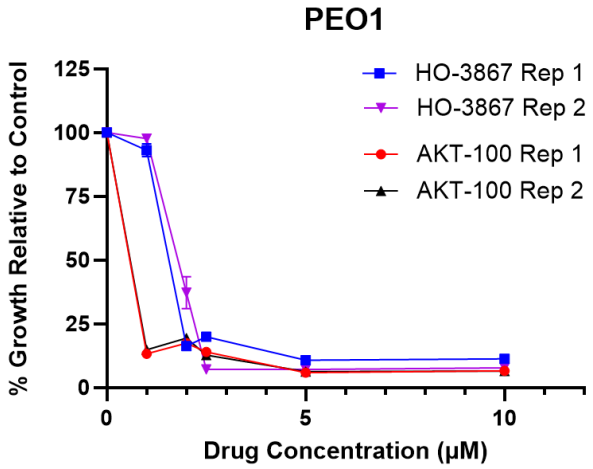

D

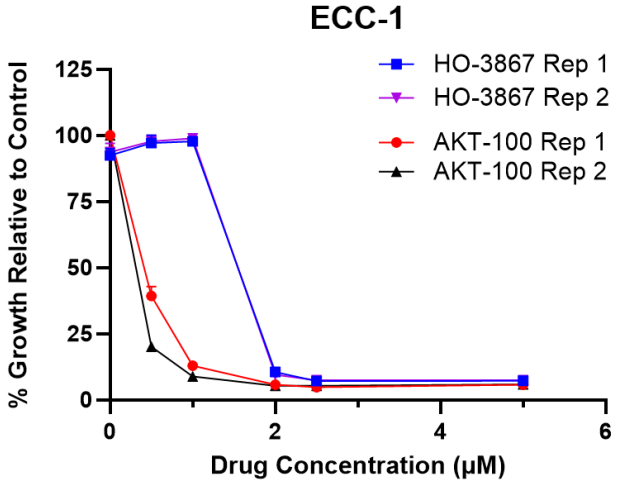

E

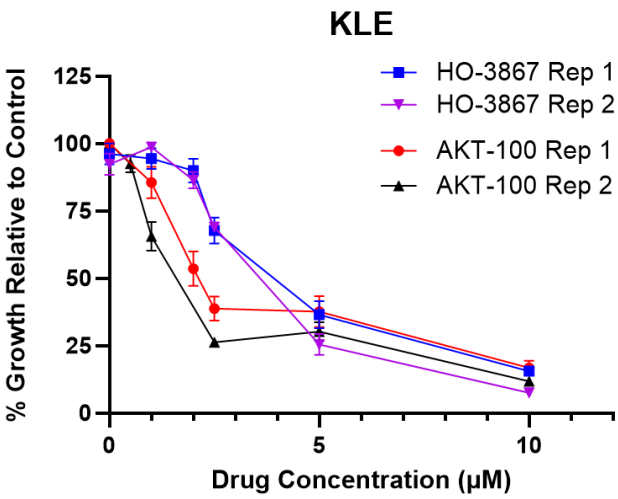

F

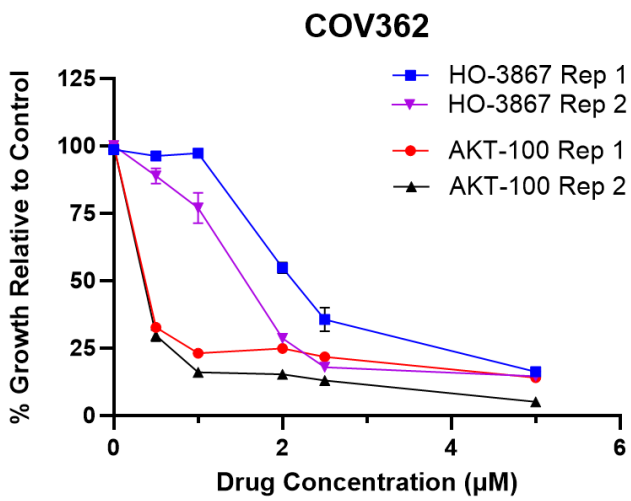

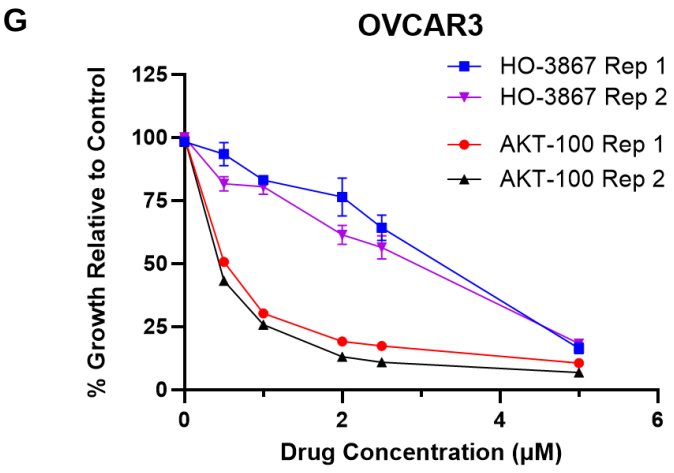

Figure 2. AKT-100 is more effective at killing cancer cells compared to HO-3867. (A) CyQUANT cell proliferation assay results of ovarian and endometrial cancer cell lines drugged for 72 hours with increasing concentrations of AKT-100. Error bars represent +/- standard error of the mean (SEM) for triplicate wells. **(B)** Table displaying the IC_{50} values obtained for each cell line treated with AKT-100 and corresponding TP53 amino acid mutations. **(C-G)** Cell proliferation assays for PE01, ECC-1, KLE, COV362 and OVCAR3 after drugging with increasing concentrations of HO-3867 versus AKT-100. Two biological replicates are shown for each cell line with each drug treatment on the same graph.

<u>AKT-111 and AKT-121 also demonstrate potential activity against cancer cells.</u>

Curcumin analogue AKT-111 was more effective at killing KLE, OVCAR3 and PEO1 cells when compared to AKT-109 and AKT-115. The calculated IC_{50} values for AKT-111 remained in the low micromolar range (3.526 μM for KLE, 2.60 μM for OVCAR3, 1.69 nM for PEO1), whereas AKT-109 and AKT-115 failed to reach an IC_{50} in our experiments (Figure 3A-C). Upon comparison of AKT-100 with AKT-121, AKT-100 again proved to be more efficient at inhibiting cell proliferation; however, the IC_{50} for AKT-121 remained in the low micromolar range as well for KLE and COV362 cells (Figure 3D-E).

A

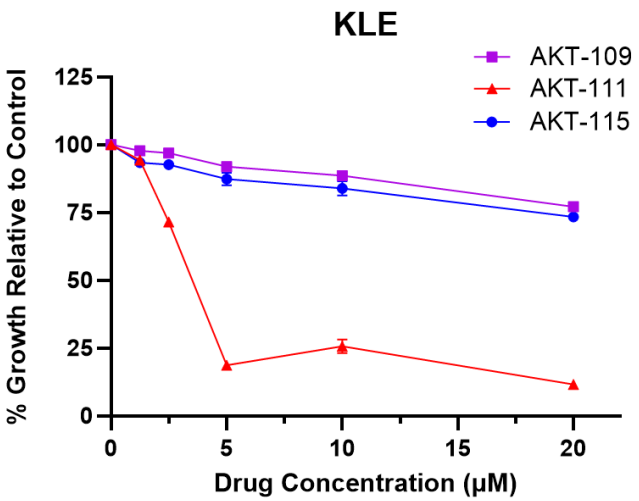
KLE
AKT-109
AKT-111
AKT-115
% Growth Relative to Control
125
100
75
50
25
0
0
5
10
15
20
Drug Concentration (μM)

B

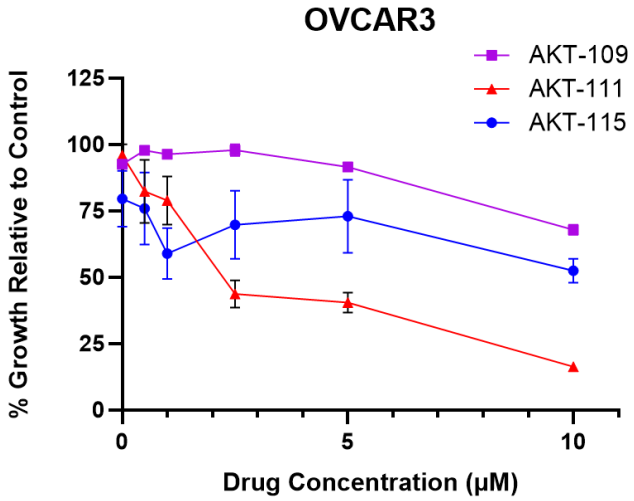
OVCAR3
AKT-109
AKT-111
AKT-115
% Growth Relative to Control
125
100
75
50
25
0
0
5
10
Drug Concentration (μM)

C

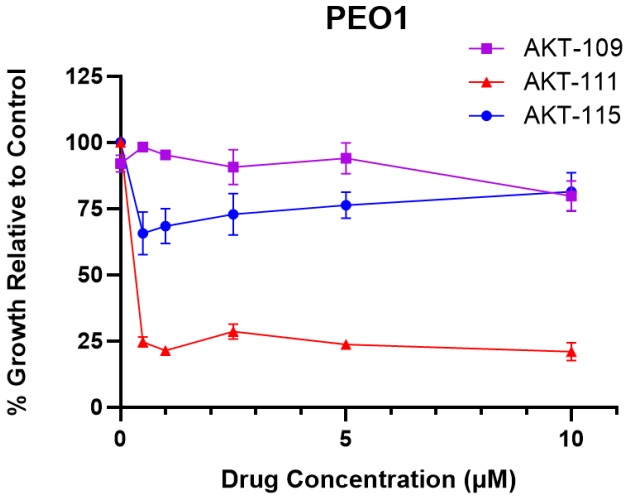
PEO1
AKT-109
AKT-111
AKT-115
% Growth Relative to Control
125
100
75
50
25
0
0
5
10
Drug Concentration (μM)

D

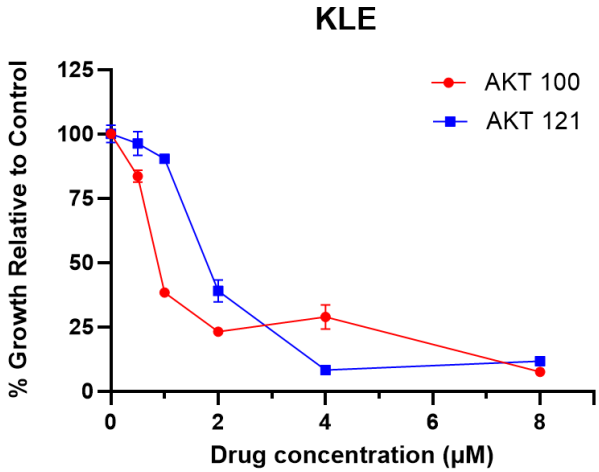
KLE
AKT 100
AKT 121
% Growth Relative to Control
125
100
75
50
25
0
0
2
4
6
8
Drug concentration (μM)

E

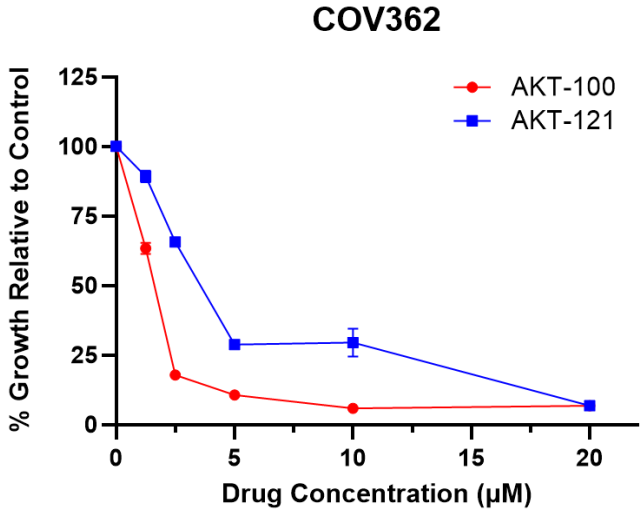
COV362
AKT-100
AKT-121
% Growth Relative to Control
125
100
75
50
25
0
0
5
10
15
20
Drug Concentration (μM)

Figure 3. AKT-111 and AKT-121 also demonstrate potential activity against cancer cells. Cell proliferation assays for **(A)** KLE **(B)** OVCAR3 and **(C)** PEO1 cells drugged with AKT derivatives AKT-109, AKT-111 and AKT-115. Cell proliferation assays for **(D)** KLE and **(E)** COV362 cells drugged with AKT-100 versus AKT-121. Error bars depict standard error of the mean for three replicate wells.

Tumor suppressive p53 transcriptional effects are reinstated after treatment with AKT-100.

KLE cells, harboring the oncogenic p53-R175H mutation, were exposed to 2.0 μM AKT-100 for 24 hours, and RNA sequencing revealed the re-enforcement of cell cycle checkpoints by the upregulation of *CDKN1A* (p21) and *GADD45* (GADD45) (Figure 4A). Proliferative signaling downstream of *ATM* (ataxia telangiectasia mutated), an important serine/threonine protein kinase stimulating cell growth, was also downregulated by AKT-100 (Figure 4A). Simultaneously, genes within the apoptotic pathway were induced that predicted for programmed cell death (Figures 4A, 4E). In our *in vitro* models, AKT-100 and HO-3867 restored wild-type tumor suppressor function in otherwise oncogenic mutant p53 by reducing cancer cell replication and promoting apoptosis. However, AKT-100 proved to be better than HO-3867 in OVCAR3 cells (Figure 4C). Figure 4B displays an increase in p21 and GADD45 in all cell lines harboring *TP53* mutations, while Figure 4D shows a decrease or no induction of DNA repair genes across these same cell lines upon treatment with AKT-100. The downregulation of the majority of genes involved in multiple DNA repair pathways (Figure 4D), with the exception of *XRCC4* and *LIG4* central to non-homologous end joining (NHEJ), portends that AKT-100 may be useful to enhance the effects of standard therapies such as PARP inhibitors and chemotherapy, as we test below.

The induction of pro-apoptotic genes is a consistent effect of curcumin analogues including AKT-100. As displayed in Figure 4E, endometrial cell lines KLE and AN3CA had an increase in apoptosis genes *BBC3* (PUMA) and *PMAIP1* (NOXA), whereas all cell lines tested increased multiple ER stress genes (*ERN1*, *XBP1*, *EIF2AK3*, *HSPA5*, *PPP1R15A*, *ATF4* and *CHOP*). Notably, prolonged ER stress activates apoptotic pathways contributing to the goal of inhibiting cancer cell proliferation (51). To understand more of the impacts of AKT-100 on additional cancer-related pathways, we report additional anti-cancer transcriptomic effects in Supplemental Figure 3.

A

KLE cells drugged with AKT-100 compared to DMSO control

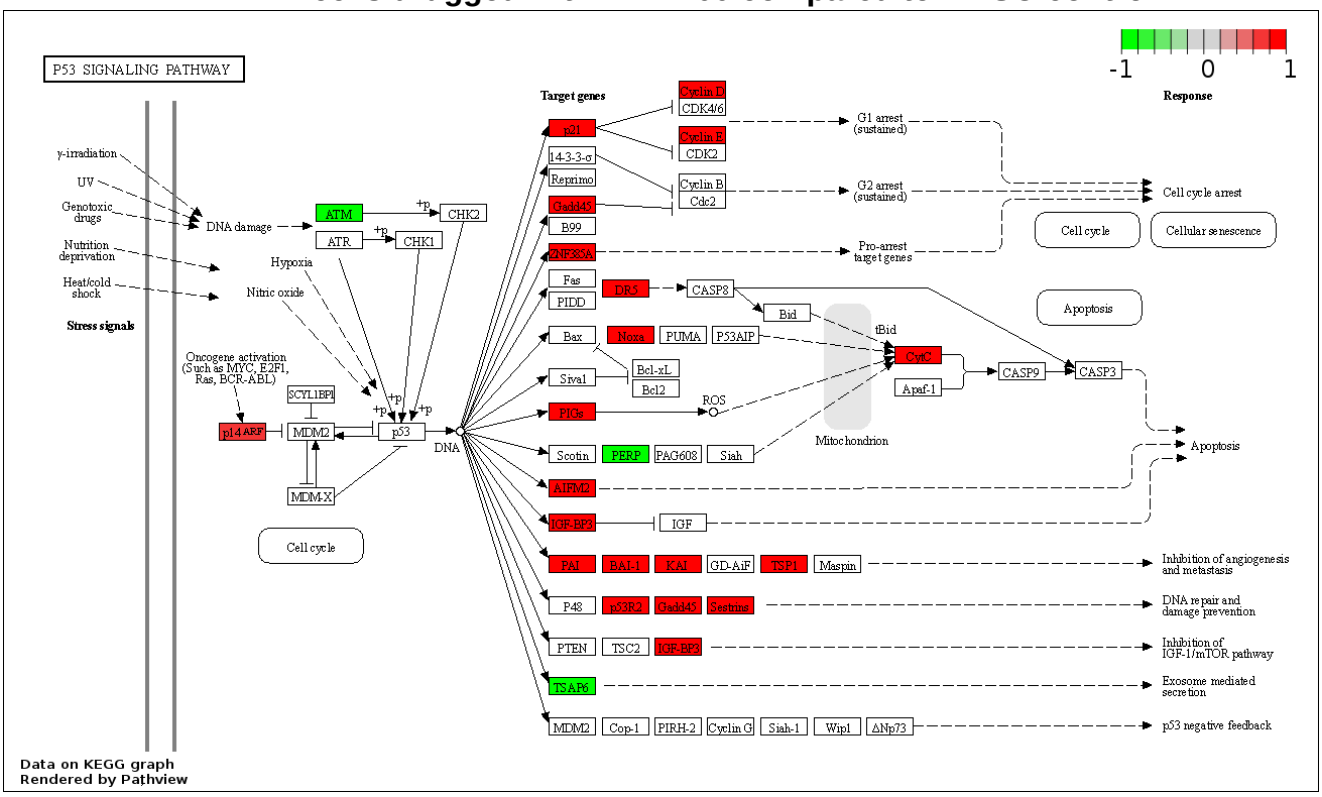

B

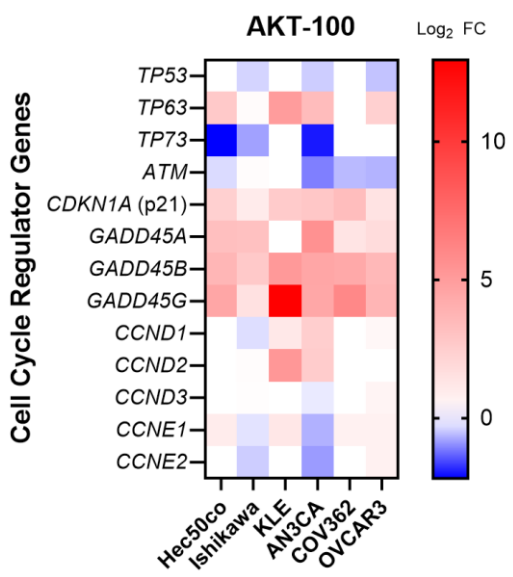

C

RNA Sequencing (24 Hours)		KLE (R175H)		COV362 (Y220C)		OVCAR3 (R248Q)	
		AKT-100	HO-3867	AKT-100	HO-3867	AKT-100	HO-3867
Protein Name	**Gene**	**Log_2 Fold Change**					
p21	*CDKN1A*	2.64	2.14	3.31	3.51	1.40	
GADD45	*GADD45A*		3.81	1.34	2.11	1.75	
	GADD45B	5.13	2.72	4.34	2.93	3.60	
	GADD45G	12.95		6.02	3.34	3.72	

D

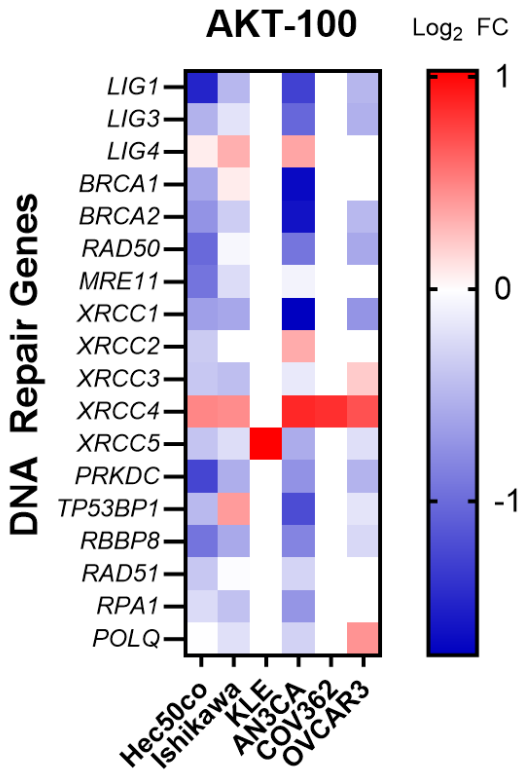

E

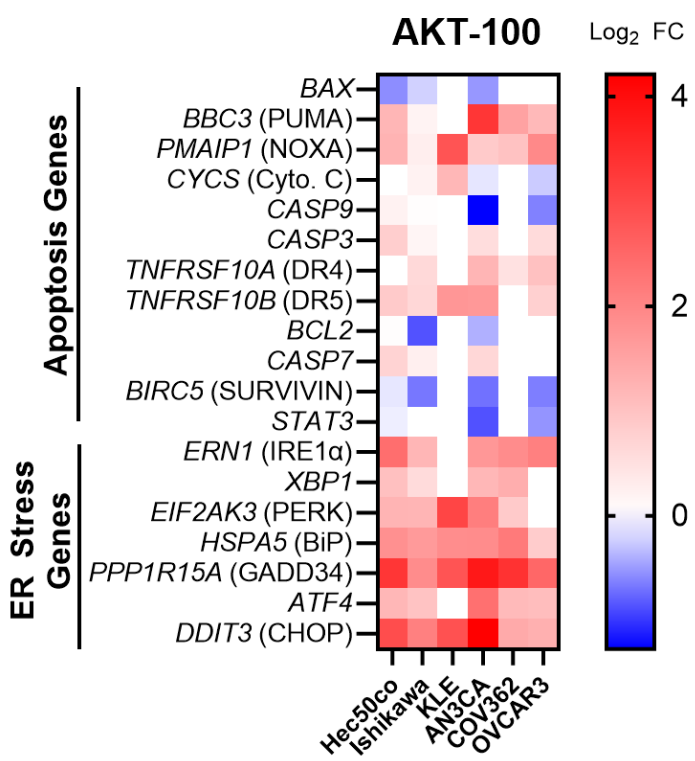

Figure 4. Tumor suppressive p53 transcriptional effects are reinstated after treatment with AKT-100. (A) Pathview analysis of RNA sequencing results in KLE cells drugged with AKT-100 showing upregulation of cell cycle regulating and apoptosis genes. Highly upregulated genes are highlighted in red and downregulated genes in green. **(B)** Heatmap displaying upregulation (red) or downregulation (blue) of cell cycle regulating genes after treatment with AKT-100 in Hec50co, Ishikawa, KLE, AN3CA, COV362 and OVCAR3 cells. **(C)** Chart comparing log_2 fold transcript change values in KLE, COV362 and OVCAR3 cells treated with AKT-100 versus HO-3867. **(D)** Heatmap displaying downregulation (blue) of most DNA repair genes after treatment with AKT-100 in Hec50co, Ishikawa, KLE, AN3CA, COV362 and OVCAR3 cells. **(E)** Heatmap displaying upregulation (red) of apoptosis and ER stress genes after treatment with AKT-100 in Hec50co, Ishikawa, KLE, AN3CA, COV362 and OVCAR3 cells. For heatmaps, the scale bars represent log_2 fold change values.

AKT-100 is synergistic with both a PARP inhibitor and with chemotherapy.

As single agents, AKT-100 and HO-3867 are effective at low µM concentrations in reducing cancer cell proliferation (Figure 2). On the other hand, we determined that the PARP inhibitor olaparib had high IC_{50} values of 10.48 µM in OVCAR3 and 65.11 µM in COV362 cells (Figures 5A, 5B, 5I), signaling PARP inhibitor resistance. Thus, we asked whether we could improve this treatment by combining it with the AKT-100 curcumin analogue. Indeed, as shown in Figure 5A, addition of 400 nM AKT-100 reduced the IC_{50} value of olaparib in combination to 4.73 µM (Figure 5I) when combined with olaparib. Also shown in Figure 5B is that addition of 20 µM constant olaparib to increasing concentrations of AKT-100 reduced the IC_{50} value of AKT-100 to 0.07 µM when used in combination. The combinatorial index was calculated to be 0.75 as shown in Figure 5I, and values less than 1 indicate synergism was achieved with combination drugging. The experiment was repeated in COV362 cells, and compared to olaparib alone, the combination with 150 nM AKT-100 significantly reduced the IC_{50} value of olaparib from 65.11 to 15.31 µM (Figure 5C). The reverse combination, with 30 µM constant olaparib added to increasing concentrations of AKT-100 reduced the AKT-100 IC_{50} value from 0.20 µM to 0.07 µM, and again the combinatorial index was 0.59, indicating synergy. Overall, these data demonstrate that the combination of olaparib and AKT-100 significantly improve cell killing compared to either agent alone, and it is possible to reduce the drug concentrations significantly and still achieve therapeutic responses. Considering that olaparib is most effective in cancers with hereditary BRCA1/BRCA2 mutations as well as in cases of tumor somatic mutations in homologous recombination repair genes, the inhibitory impact of AKT-100 on genes involved in homologous recombination shown in Figure 4D likely underlies the synergy when combined with olaparib, basically creating cancer cell homologous recombination repair deficiency.

We next asked whether other chemotherapeutic regiments such as paclitaxel and carboplatin, that induce DNA damage, are also synergistic with AKT-100. We tested KLE cells with paclitaxel and determined the IC_{50} to be 30.08 nM, but addition of 2 µM AKT-100 reduced this value to 0.50 nM (Figures 5E, 5I). The reverse combination showed the IC_{50} for AKT-100 alone was 1.04 µM, however addition of only 10 nM of constant paclitaxel dropped the IC_{50} of AKT-100 10-fold to 0.10 µM (Figures 5F, 5I). The combinatorial index was calculated to be 0.11 - well below 1 (Figure 5I). As for combination drugging with carboplatin, we again determined it to be synergistic in KLE cells which harbor the most resistant p53 R175H mutation. Treatment

with carboplatin alone demonstrated an IC_{50} of 1.72 µM, and addition of 2 µM AKT-100 reduced this to 0.1027 nM (Figures 5G, 5I). The reverse combination determined an IC_{50} with AKT-100 alone to be 1.32 µM and combination with 2 µM carboplatin reduced it to 0.15 µM (Figure 5H, 5I). The combinatorial index was calculated to be 0.11 (Figure 5I), demonstrating significant synergy between AKT-100 and carboplatin.

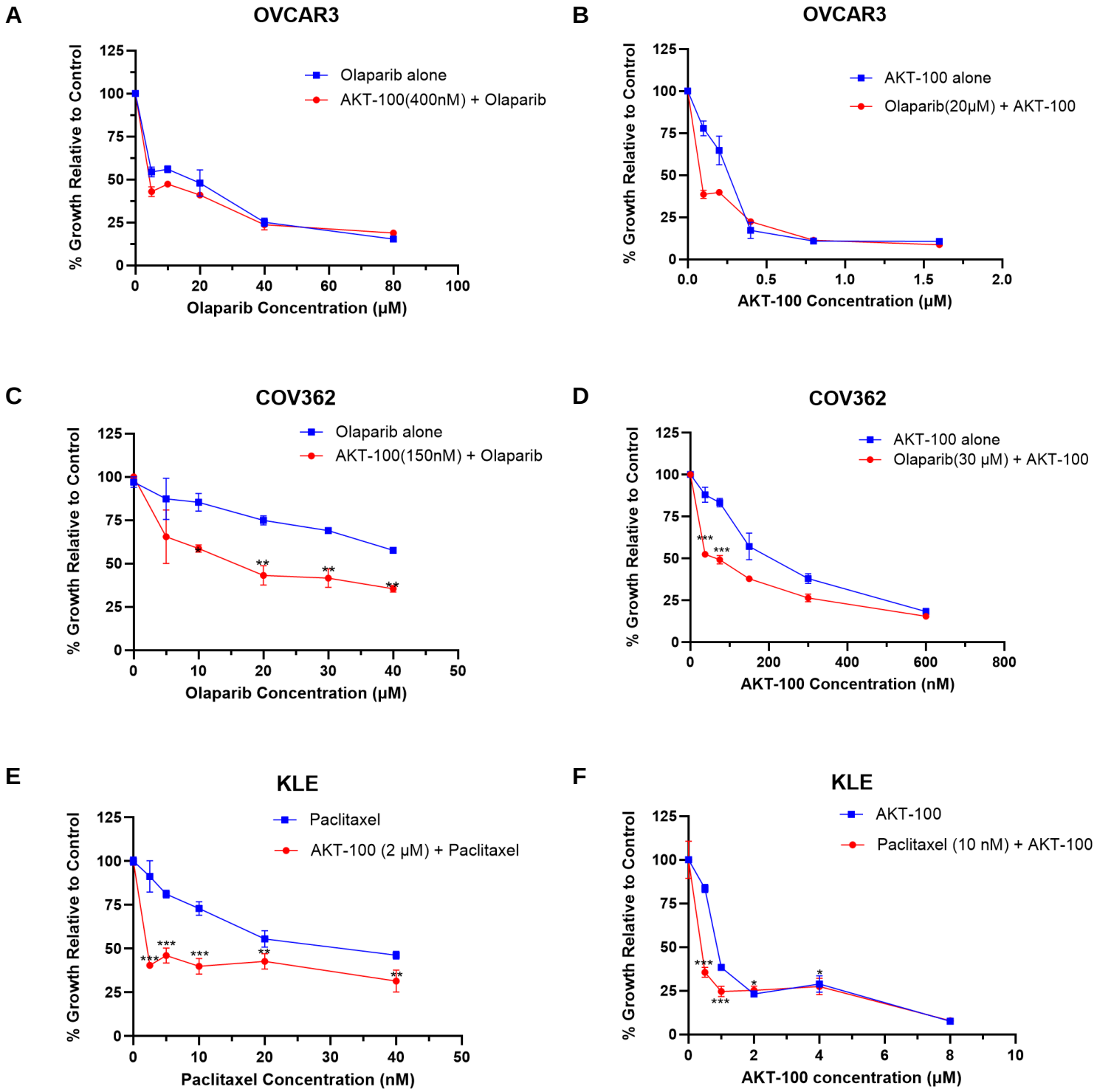

G

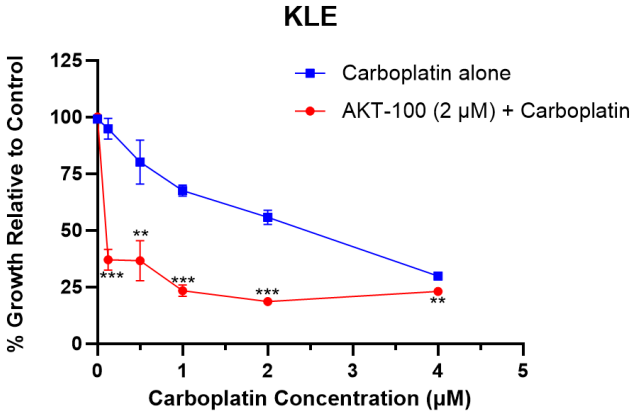

H

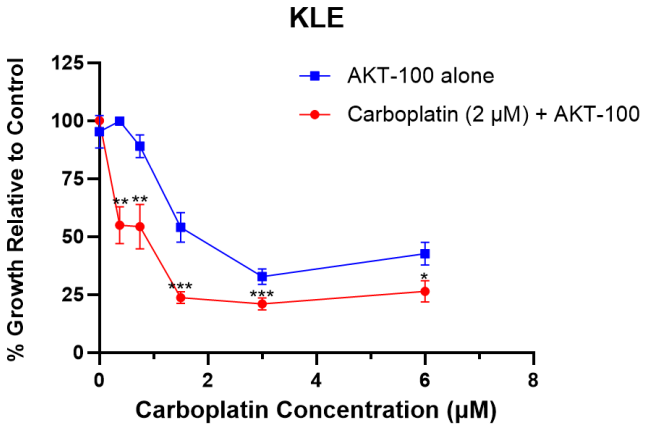

I

Cell Line (TP53 Mutation)	Drug Treatment	IC_{50} Value	R^2 Value	Combinatorial Index (CI)
OVCAR3 (R248Q)	Olaparib alone	10.48 μM	0.9219	**0.75**
	AKT-100 alone	0.23 μM	0.9390	
	AKT-100 (400 nM) + Olaparib	4.73 μM	0.9566	
	Olaparib (20 μM) + AKT-100	0.07 μM	0.9791	
COV362 (Y220C)	Olaparib alone	65.11 μM	0.7022	**0.59**
	AKT-100 alone	0.20 μM	0.9547	
	AKT-100 (150 nM) + Olaparib	15.31 μM	0.8163	
	Olaparib (30 μM) + AKT-100	0.07 μM	0.9275	
KLE (R175H)	AKT-100 alone	1.04 μM	0.9148	**0.17**
	Paclitaxel alone	30.08 nM	0.9494	
	AKT-100 (2 μM) + Paclitaxel	0.50 nM	0.9499	
	Paclitaxel (10 nM) + AKT-100	0.10 μM	0.9489	
KLE (R175H)	Carboplatin alone	1.72 μM	0.9816	**0.11**
	AKT-100 alone	1.32 μM	0.8435	
	AKT-100 (2 μM) + Carboplatin	0.1027 nM	0.9384	
	Carboplatin (2 μM) + AKT-100	0.15 μM	0.9459	

Figure 5. AKT-100 is synergistic with both a PARP inhibitor and with chemotherapy. (A) Growth inhibition curves in OVCAR3 cells comparing olaparib alone versus olaparib with 400 nM AKT-100. **(B)** Cell proliferation assay displaying OVCAR3 cells drugged with AKT-100 alone compared to AKT-100 plus constant 20 μM olaparib. **(C)** Cell proliferation assay displaying COV362 cells drugged with olaparib alone versus olaparib with 150 nM AKT-100. **(D)** Proliferation assay comparing AKT-100 alone versus AKT-100 plus 30 μM olaparib in COV362 cells. **(E)** KLE cells were treated with paclitaxel alone versus paclitaxel plus 2 μM constant AKT-100 or **(F)** AKT-100 alone compared to AKT-100 with 10 nM paclitaxel. **(G)** Proliferation assay in KLE cells treated with carboplatin alone or carboplatin with 2 μM constant AKT-100. **(H)** Graph comparing cell proliferation of KLE cells treated with either AKT-100 alone versus AKT-100 with 2 μM carboplatin. **(I)** Table listing the combination drug treatments in OVCAR3, COV362, and KLE cells treated with chemotherapy drugs and AKT-100. Listed are determined IC_{50} values, R^2 values and calculated combinatorial indices. For A-H, single drug treatments are blue lines and combination treatments are red lines. Unpaired t-tests were performed to compare the two groups, and statistical significance is indicated as follows: *, $p < 0.05$; **, $p < 0.01$; ***, $p < 0.001$.

Discussion

Despite the overall improvement in outcomes for many cancer patients today, women suffer from increased year over year incidences (52) and deaths (53) from uterine endometrial cancer up to the current decade. Ovarian cancer, now understood to arise primarily in the epithelium of the fallopian tube and to spread early in the process of oncogenesis, is often lethal with fewer than 50% of patients surviving 5 years after diagnosis (54). A common thread among these malignancies is the inactivation of the central tumor suppressor p53, mostly through mutation. We and others have evaluated the rate of the various types of mutations in the p53 gene, *TP53*, and found that approximately 70 percent result in single amino acid hotspot alterations in the DNA binding domain of p53, preventing its normal pro-apoptotic and DNA repair transcriptional activity, while enhancing some mutant p53 functions that encourage oncogenesis and tumor progression (55). Recurrent mutations found in nearly all types of cancers include R175H, R248Q/W, Y220C, R273H/C, R282W, G245S, R249S. Many of the recurrent missense mutations occur at methylated CpG sites which encode arginine residues that contact the DNA and are conserved over evolutionary scales (4).

Indeed, considering comparative biology and evolution, the critical importance of functional, WT p53 in cancer prevention and longevity is emphasized when studying other animals that are resistant to cancer and live longer than expected lives (2). These include elephants and bats, with genomes encoding multiple p53 genes – 20 copies of *TP53* are encoded in the elephant genome, and two copies of *TP53* exist in the bat genome compared to a single copy in most species including humans. The frequent mutation of *TP53* creates individual and species vulnerabilities to cancer; however, could there be a therapeutic mechanism to reverse or prevent such mutations and to enhance a longer and healthier lifespan? The goal of our research is to develop such a strategy.

The molecular properties of curcumin as an anti-inflammatory, anti-oxidant, anti-angiogenic and anti-cancer agent have been the subject of investigations over decades, as summarized by Vander Jagt *et al*. (25). One of the most important observations has been the identification of p53 as a target for the curcumin analogue HO-3867 (22, 40). This supports the likelihood that curcumin and its analogues may serve as p53 reactivators with the potential to bind to mutant forms of p53 to recapitulate wild type pro-apoptotic activity in cancer cells. Yet to date, despite several p53 reactivator therapeutic molecules being extensively assessed in

preclinical studies, such as HO-3867, and two therapeutics, APR-246 and PC14586, in clinical trials (56, 57), none has yet been approved for clinical use. Nevertheless, the potent anticancer activity of such agents continues to bode well for the eventual development and use of curcumin analogues in medicine.

In these studies, we report the activity of AKT-100, a novel derivative of HO-3867 and a curcumin analogue as an anticancer therapeutic with single agent activity. We demonstrate the substantial impact of relatively low concentrations of AKT-100 on cell viability using multiple cell models of advanced gynecologic cancer with mutant forms of p53. Our data confirm that mutant p53 proteins are bound by AKT-100, and that this results in the re-establishment of wild type p53 transcriptional effects including the induction of apoptotic genes and the inhibition of multiple cancer cell DNA repair pathways. Potentially as a result of the inhibition of these DNA repair pathways, AKT-100 is synergistic with the PARP inhibitor olaparib and with paclitaxel and carboplatin, the standard chemotherapeutic agents used to treat p53 mutant and other advanced forms of endometrial and ovarian cancers. The opportunity to prevent resistance to chemotherapy and to PARP inhibitors using a curcumin analogue is highly clinically relevant (58). Additionally, a strength of the work reported herein is the identification of a novel curcumin analogue that binds to mutant forms of p53 with the potential to reactivate the WT p53 transcriptome. We and others have proposed that reactivating the normal, pro-apoptotic effects of WT p53 in tumor cells harboring mutant forms of p53 can have substantial clinical benefit for patients with advanced cancers. Nevertheless, given the reported therapeutic impact of curcumin analogues in diseases ranging from cancer to arthritis to Alzheimer's disease, multiple mechanisms of action are highly likely and should be delineated in follow-up studies (29). Other targets, including STAT3, as reported to be an additional target of HO-3867 beyond p53 (59), are likely to be involved in the activity of AKT-100 and other curcumin analogues, and these targets should be more fully defined. In addition, identifying curcumin analogues in future studies with a higher affinity for multiple mutant forms of p53 compared to WT would be advantageous (16). With the accomplishment of these goals, the future may hold the promise of synthesizing different curcumin analogues with activities tailored to inhibit targets promoting cancer as well as other diseases.

Acknowledgements

This work was supported by the following grants: 5R01CA99908–22 (KL), CDMRP CA210610 (KL), CDMRP CA2220729 (KL), P50CA264793 (KL), P01CA872735 (KL), The University of New Mexico Comprehensive Cancer Center (UNMCCC) P30CA118100, with support from the UNMCCC Biostatistics and the ATG Genomics Shared Resources.

Authorship contribution statement

Geneva Williams: Writing – original draft, Methodology, Investigation, Formal analysis, Data curation. **Lane E. Smith, Jamie L. Padilla, Alexander Goss, Daisy Belmares-Ortega, Xiangxiang Wu, Jennifer N. Daw, Prakash Jagtap:** Methodology, Investigation, Data curation. **Jun-yong Choe:** Methodology, Investigation, Formal analysis, Manuscript development. **Sumegha Mitra**: Writing - review and editing of the manuscript. **Kimberly K. Leslie:** Writing – review & editing, Writing – original draft, Validation, Supervision, Resources, Project administration, Methodology, Investigation, Funding acquisition, Formal analysis, Data curation, Conceptualization.

Declaration of competing interest

The authors declare that they have no known competing financial interests or personal relationships that could have appeared to influence the work reported in this paper.

References

1. Bartek J, Bartkova J, Vojtesek B, Staskova Z, Lukas J, Rejthar A, et al. Aberrant expression of the p53 oncoprotein is a common feature of a wide spectrum of human malignancies. Oncogene. 1991;6(9):1699–703.
2. Levine AJ. p53: 800 million years of evolution and 40 years of discovery. Nat Rev Cancer. 2020;20(8):471–80.
3. Aubrey BJ, Kelly GL, Janic A, Herold MJ, Strasser A. How does p53 induce apoptosis and how does this relate to p53-mediated tumour suppression? Cell Death Differ. 2018;25(1):104–13.
4. Baugh EH, Ke H, Levine AJ, Bonneau RA, Chan CS. Why are there hotspot mutations in the TP53 gene in human cancers? Cell Death Differ. 2018;25(1):154–60.
5. Leslie KK, Filiaci VL, Mallen AR, Thiel KW, Devor EJ, Moxley K, et al. Mutated p53 portends improvement in outcomes when bevacizumab is combined with chemotherapy in advanced/recurrent endometrial cancer: An NRG Oncology study. Gynecol Oncol. 2021;161(1):113–21.
6. Thiel KW, Devor EJ, Filiaci VL, Mutch D, Moxley K, Alvarez Secord A, et al. TP53 Sequencing and p53 Immunohistochemistry Predict Outcomes When Bevacizumab Is Added to Frontline Chemotherapy in Endometrial Cancer: An NRG Oncology/Gynecologic Oncology Group Study. J Clin Oncol. 2022;40(28):3289–300.
7. Marei HE, Althani A, Afifi N, Hasan A, Caceci T, Pozzoli G, et al. p53 signaling in cancer progression and therapy. Cancer Cell Int. 2021;21(1):703.

8. Agupitan AD, Neeson P, Williams S, Howitt J, Haupt S, Haupt Y. P53: A Guardian of Immunity Becomes Its Saboteur through Mutation. Int J Mol Sci. 2020;21(10).
9. Haupt S, Raghu D, Haupt Y. Mutant p53 Drives Cancer by Subverting Multiple Tumor Suppression Pathways. Frontiers in oncology. 2016;6:12.
10. Willis A, Jung EJ, Wakefield T, Chen X. Mutant p53 exerts a dominant negative effect by preventing wild-type p53 from binding to the promoter of its target genes. Oncogene. 2004;23(13):2330–8.
11. Garritano S, Inga A, Gemignani F, Landi S. More targets, more pathways and more clues for mutant p53. Oncogenesis. 2013;2(7):e54.
12. Bullock AN, Henckel J, DeDecker BS, Johnson CM, Nikolova PV, Proctor MR, et al. Thermodynamic stability of wild-type and mutant p53 core domain. Proc Natl Acad Sci U S A. 1997;94(26):14338–42.
13. Freed-Pastor WA, Prives C. Mutant p53: one name, many proteins. Genes Dev. 2012;26(12):1268–86.
14. Muller PA, Vousden KH. Mutant p53 in cancer: new functions and therapeutic opportunities. Cancer Cell. 2014;25(3):304–17.
15. Integrated genomic analyses of ovarian carcinoma. Nature. 2011;474(7353):609–15.
16. Stegh AH. Targeting the p53 signaling pathway in cancer therapy - the promises, challenges and perils. Expert Opin Ther Targets. 2012;16(1):67–83.
17. Ravi R, Mookerjee B, Bhujwalla ZM, Sutter CH, Artemov D, Zeng Q, et al. Regulation of tumor angiogenesis by p53-induced degradation of hypoxia-inducible factor 1alpha. Genes Dev. 2000;14(1):34–44.
18. Xu-Monette ZY, Zhang M, Li J, Young KH. PD-1/PD-L1 Blockade: Have We Found the Key to Unleash the Antitumor Immune Response? Front Immunol. 2017;8:1597.
19. Liu S, Liu T, Jiang J, Guo H, Yang R. p53 mutation and deletion contribute to tumor immune evasion. Front Genet. 2023;14:1088455.
20. Eskander RN, Sill MW, Beffa L, Moore RG, Hope JM, Musa FB, et al. Pembrolizumab plus Chemotherapy in Advanced Endometrial Cancer. N Engl J Med. 2023;388(23):2159–70.
21. Mirza MR, Chase DM, Slomovitz BM, dePont Christensen R, Novak Z, Black D, et al. Dostarlimab for Primary Advanced or Recurrent Endometrial Cancer. N Engl J Med. 2023;388(23):2145–58.
22. Madan E, Parker TM, Bauer MR, Dhiman A, Pelham CJ, Nagane M, et al. The curcumin analog HO-3867 selectively kills cancer cells by converting mutant p53 protein to transcriptionally active wildtype p53. J Biol Chem. 2018;293(12):4262–76.
23. Mast JM, Tse D, Shee K, Lakshmi Kuppusamy M, Kmiec MM, Kalai T, et al. Diarylidenylpiperidones, H-4073 and HO-3867, Induce G2/M Cell-Cycle Arrest, Apoptosis and Inhibit STAT3 Phosphorylation in Human Pancreatic Cancer Cells. Cell Biochem Biophys. 2019;77(2):109–19.
24. Selvendiran K, Ahmed S, Dayton A, Kuppusamy ML, Rivera BK, Kalai T, et al. HO-3867, a curcumin analog, sensitizes cisplatin-resistant ovarian carcinoma, leading to therapeutic synergy through STAT3 inhibition. Cancer Biol Ther. 2011;12(9):837–45.
25. Weber WM, Hunsaker LA, Abcouwer SF, Deck LM, Vander Jagt DL. Anti-oxidant activities of curcumin and related enones. Bioorg Med Chem. 2005;13(11):3811–20.
26. Kaur K, Al-Khazaleh AK, Bhuyan DJ, Li F, Li CG. A Review of Recent Curcumin Analogues and Their Antioxidant, Anti-Inflammatory, and Anticancer Activities. Antioxidants (Basel). 2024;13(9).
27. Qudjani E, Iman M, Davood A, Ramandi MF, Shafiee A. Design and Synthesis of Curcumin-Like Diarylpentanoid Analogues as Potential Anticancer Agents. Recent Pat Anticancer Drug Discov. 2016;11(3):342–51.
28. Noureddin SA, El-Shishtawy RM, Al-Footy KO. Curcumin analogues and their hybrid molecules as multifunctional drugs. Eur J Med Chem. 2019;182:111631.
29. Amalraj A, Pius A, Gopi S, Gopi S. Biological activities of curcuminoids, other biomolecules from turmeric and their derivatives - A review. J Tradit Complement Med. 2017;7(2):205–33.
30. Li H, Liu ZY, Wu N, Chen YC, Cheng Q, Wang J. PARP inhibitor resistance: the underlying mechanisms and clinical implications. Mol Cancer. 2020;19(1):107.
31. Linke SP, Sengupta S, Khabie N, Jeffries BA, Buchhop S, Miska S, et al. p53 interacts with hRAD51 and hRAD54, and directly modulates homologous recombination. Cancer Res. 2003;63(10):2596–605.
32. Williams AB, Schumacher B. p53 in the DNA-Damage-Repair Process. Cold Spring Harb Perspect Med. 2016;6(5).
33. Flint AL, Hansen DW, Brown LD, Stewart LE, Ortiz E, Panda SS. Modified Curcumins as Potential Drug Candidates for Breast Cancer: An Overview. Molecules. 2022;27(24).

34. Ayed A, Mulder FA, Yi GS, Lu Y, Kay LE, Arrowsmith CH. Latent and active p53 are identical in conformation. Nat Struct Biol. 2001;8(9):756–60.
35. Liu H, Naismith JH. An efficient one-step site-directed deletion, insertion, single and multiple-site plasmid mutagenesis protocol. BMC Biotechnol. 2008;8:91.
36. Miroux B, Walker JE. Over-production of proteins in Escherichia coli: mutant hosts that allow synthesis of some membrane proteins and globular proteins at high levels. J Mol Biol. 1996;260(3):289–98.
37. Vedadi M, Niesen FH, Allali-Hassani A, Fedorov OY, Finerty PJ, Jr., Wasney GA, et al. Chemical screening methods to identify ligands that promote protein stability, protein crystallization, and structure determination. Proc Natl Acad Sci U S A. 2006;103(43):15835–40.
38. Nettleship JE, Brown J, Groves MR, Geerlof A. Methods for protein characterization by mass spectrometry, thermal shift (ThermoFluor) assay, and multiangle or static light scattering. Methods Mol Biol. 2008;426:299–318.
39. King AC, Woods M, Liu W, Lu Z, Gill D, Krebs MR. High-throughput measurement, correlation analysis, and machine-learning predictions for pH and thermal stabilities of Pfizer-generated antibodies. Protein Sci. 2011;20(9):1546–57.
40. Smith LE, Padilla JL, Licor A, Steinkamp MP, Lagutina IV, Guo Y, et al. Novel p53 reactivators that are synergistic with olaparib for the treatment of gynecologic cancers with mutant p53. Transl Oncol. 2025;61:102522.
41. Lipinski CA. Lead- and drug-like compounds: the rule-of-five revolution. Drug Discov Today Technol. 2004;1(4):337–41.
42. Doak BC, Kihlberg J. Drug discovery beyond the rule of 5 - Opportunities and challenges. Expert Opin Drug Discov. 2017;12(2):115–9.
43. Lipinski CA, Lombardo F, Dominy BW, Feeney PJ. Experimental and computational approaches to estimate solubility and permeability in drug discovery and development settings. Adv Drug Deliv Rev. 2001;46(1-3):3–26.
44. Wiseman T, Williston S, Brandts JF, Lin LN. Rapid measurement of binding constants and heats of binding using a new titration calorimeter. Anal Biochem. 1989;179(1):131–7.
45. Demarse NA, Quinn CF, Eggett DL, Russell DJ, Hansen LD. Calibration of nanowatt isothermal titration calorimeters with overflow reaction vessels. Anal Biochem. 2011;417(2):247–55.
46. Huynh K, Partch CL. Analysis of protein stability and ligand interactions by thermal shift assay. Curr Protoc Protein Sci. 2015;79:28 9 1– 9 14.
47. Chen RF, Cohen PF. Quenching of tyrosine fluorescence in proteins by phosphate. Arch Biochem Biophys. 1966;114(3):514–22.
48. Eftink MR, Ghiron CA. Fluorescence quenching studies with proteins. Anal Biochem. 1981;114(2):199–227.
49. Giancotti V, Quadrifoglio F, Cowgill RW, Crane-Robinson C. Fluorescence of buried tyrosine residues in proteins. Biochim Biophys Acta. 1980;624(1):60–5.
50. Calhoun DB, Vanderkooi JM, Holtom GR, Englander SW. Protein fluorescence quenching by small molecules: protein penetration versus solvent exposure. Proteins. 1986;1(2):109–15.
51. Verfaillie T, Garg AD, Agostinis P. Targeting ER stress induced apoptosis and inflammation in cancer. Cancer Lett. 2013;332(2):249–64.
52. Lortet-Tieulent J, Ferlay J, Bray F, Jemal A. International Patterns and Trends in Endometrial Cancer Incidence, 1978-2013. J Natl Cancer Inst. 2018;110(4):354–61.
53. Jemal A, Ward EM, Johnson CJ, Cronin KA, Ma J, Ryerson B, et al. Annual Report to the Nation on the Status of Cancer, 1975-2014, Featuring Survival. J Natl Cancer Inst. 2017;109(9).
54. SEER*Explorer: An interactive website for SEER cancer statistics. https://seer.cancer.gov/statistics-network/explorer/: Surveillance Research Program, National Cancer Institute; 2023 [
55. Olivier M, Hollstein M, Hainaut P. TP53 mutations in human cancers: origins, consequences, and clinical use. Cold Spring Harb Perspect Biol. 2010;2(1):a001008.
56. Hu J, Cao J, Topatana W, Juengpanich S, Li S, Zhang B, et al. Targeting mutant p53 for cancer therapy: direct and indirect strategies. J Hematol Oncol. 2021;14(1):157.
57. Papavassiliou KA, Vassiliou AG, Papavassiliou AG. Rezatapopt: A promising small-molecule "refolder" specific for TP53(Y220C) mutant tumors. Neoplasia. 2025;67:101201.

58. Dias MP, Moser SC, Ganesan S, Jonkers J. Understanding and overcoming resistance to PARP inhibitors in cancer therapy. Nat Rev Clin Oncol. 2021;18(12):773–91.
59. Rath KS, Naidu SK, Lata P, Bid HK, Rivera BK, McCann GA, et al. HO-3867, a safe STAT3 inhibitor, is selectively cytotoxic to ovarian cancer. Cancer Res. 2014;74(8):2316–27.